Time evolution of tetragonal-orthorhombic ferroelastics

S. H. Curnoe* and A. E. Jacobs†
Department of Physics, University of Toronto, Toronto, Ontario, Canada M5S 1A7
(Received 14 December 2000; published 17 July 2001)

We study numerically the time evolution of two-dimensional (2D) domain patterns in proper tetragonal-orthorhombic (T-O) ferroelastics. Our equations of motion are derived from classical elasticity theory, augmented by nonlinear and strain-gradient terms. Our results differ from those found by other dynamical methods. We study first the growth of the 2D nucleus resulting from homogeneous nucleation events. The later shape of the nucleus is largely independent of how it was nucleated. In soft systems, the nucleus forms a flowerlike pattern. In stiff systems, which seem to be more realistic, it forms an X shape with twinned arms in the 110 and $\bar{1}10$ directions. Second, we study the relaxation that follows completion of the phase transition; at these times, the T phase has disappeared and both O variants are present, separated by walls preferentially in 110-type planes. We observe a variety of coarsening mechanisms, most of them counterintuitive. Our patterns are strikingly similar to those observed in transmission electron microscopy of the improper T-O ferroelastic $YBa_2Cu_3O_7$.

DOI: 10.1103/PhysRevB.64.064101 PACS number(s): 81.30.Kf, 68.35.−p, 62.20.Dc

I. INTRODUCTION

Ferroelastics[1,2] are crystalline solids that undergo a shape-changing phase transition, usually first order, to a state of lower symmetry with decreasing temperature T. A prominent example is the tetragonal-orthorhombic (T-O) ferroelastic $YBa_2Cu_3O_7$.[2,3] At the transition temperature T_c, the unit cell of the parent (high-T) phase distorts spontaneously in one of several equivalent directions. Each of these degenerate distortions corresponds to a differently oriented *variant* of the product (low-T) phase. Below T_c, all variants are usually present, separated from each other by domain walls with preferred orientations. Domain patterns in ferroelastics differ greatly from those in ferromagnets, gainsaying the analogy responsible for the very name ferroelastic[1] and confounding intuition based on conventional order-parameter systems. In the final analysis, ferroelastic patterns are different because the strains are not independent order parameters but rather are linked by compatibility relations.

The theory of proper ferroelastics (where the strain is the primary order parameter) extends the classical theory of elastic continua by adding higher-order terms in the strains and also derivatives of the strains. This strain-only theory was first used[4] in one dimension (1D); its first important result was a remarkable solution[5] for the twin wall of cubic-tetragonal (C-T) materials. It has since been used to study various aspects of (i) T-O materials,[6–12] (ii) the 1D problem,[13] (iii) cubic-tetragonal (C-T) materials,[14–16] and (iv) hexagonal-orthorhombic (H-O) and related materials.[17] Although the strain-only theory applies strictly only to proper ferroelastics, it has nevertheless succeeded in explaining a wide variety of domain patterns also in improper T-O (Ref. 12) and H-O (Ref. 17) materials. A much larger literature (examples are Refs. 18–24) includes order parameters in addition to the strains or applies more phenomenological approaches.

No consensus exists regarding the description of ferroelastic dynamics. Our equations of motion are based on classical elasticity theory;[25] this formalism has been used only infrequently, to study 1D,[13] C-T,[14] and H-O (Refs. 17 and 26) systems. Fundamentally different dynamical schemes were used in the strain-only theories of Refs. 7,9–11,15, and 21, often only as a tool to find static structures.

The following presents the application of the classical equations of motion[25] to the dynamics of proper T-O ferroelastics. The study was motivated in part by the electron-microscopy results[2,3] available for $YBa_2Cu_3O_7$; this is an improper material (the orthorhombic distortion is a secondary effect of the oxygen ordering), but the success of the static strain-only theory[12] for $YBa_2Cu_3O_7$ warrants an extension to the dynamics. Computational resources allow us to consider only 2D structures, with possible application to thin films, particularly to the patterns of Refs. 2 and 3.

The paper is organized as follows. Section II gives the expression for the T-O strain energy in 2D and then finds the equations of motion. We distinguish between soft and stiff systems according to the energy cost for wall directions off optimal. The strain-only theory predicts softening with decreasing T, perhaps with observable consequences. Section III applies this formalism to investigate the growth of O nuclei from the supercooled T phase. We find that the developed nuclei are largely independent of the nucleation mechanism; in both soft and stiff systems they differ markedly from the nuclei in other theories.[11,22] In soft systems, nuclei are flowerlike; they simply expand without generating much additional structure. In stiff systems, they form an X shape with twinned arms in the major growth directions (110 and $\bar{1}10$); additional structure forms near the center and propagates outward along the arms. Section IV examines the coarsening mechanisms that follow completion of the phase transition, including domain-wall merges, formation, and disappearance of island domains, rank formation of ribbon tips and their coordinated retraction, and tip splitting (in stiff systems). Section V provides a summary and proposals for further investigations.

II. EQUATIONS OF MOTION

A. Expansion of the strain energy

The energy of proper ferroelastics is expressed solely in terms of the strains. These are combinations of derivatives of the displacement $\mathbf{u}(\mathbf{x})$ of a material point from its position $\mathbf{x}$ in the high-T symmetric phase. We discuss only structures uniform in the tetragonal fourfold (x_3) direction. We define the three strains in 2D by

$$e_1=(\eta_{11}+\eta_{22})/\sqrt{2}, \tag{1a}$$

$$e_2=(\eta_{11}-\eta_{22})/\sqrt{2}, \tag{1b}$$

$$e_3=(\eta_{12}+\eta_{21})/2, \tag{1c}$$

where the components of the strain tensor η are

$$\eta_{ij}=\frac{1}{2}(u_{i,j}+u_{j,i}+u_{k,i}u_{k,j}); \tag{2}$$

here $u_{i,j}=\partial u_i/\partial x_j=\partial_j u_i$ and repeated indices are summed. All three strains vanish in the T phase. The deviatoric strain e_2 is the primary order parameter of the T-O transformation. In the lowest-energy product state, e_2 takes one of two degenerate values $\pm e_{20}$ corresponding to a stretch in either the x_1 or the x_2 direction. The dilatational and shear strains e_1 and e_3 vanish for these two states, and also for twin bands,[6] but not for the complex domain patterns formed by colliding bands.

At this stage in the theory of ferroelastics, one wants to examine the simplest possible form for the energy density $\mathcal{F}$, to include only those terms required by symmetry, for stability, and to explain experiments. This simplest form is

$$\mathcal{F}=\frac{1}{2}[A_1e_1^2+A_2(T)e_2^2+A_3e_3^2]+\frac{B_2}{4}e_2^4+\frac{C_2}{6}e_2^6 + \frac{d_2}{2}(\nabla e_2)^2; \tag{3}$$

all terms are invariant under the symmetry operations of the T group. The dilatational, deviatoric, and shear stiffnesses A_1, $A_2(T)$ and A_3 in the first term are related to the elastic constants. Stability requires $A_1\geqslant 0$ and $A_3\geqslant 0$. But $A_2(T)$ softens with decreasing T, as $A_2(T)=a(T-T_0)$, and the T phase is unstable for $T<T_0$. To describe the phase transition, we need the terms in e_2^4 and e_2^6; we assume a first-order transition ($B_2<0$), and so $C_2>0$ for stability. At high T, namely $A_2(T)>B_2^2/4C_2$, only the T minimum exists. At lower T, two O minima occur at $e_2=\pm e_{20}(T)$, where

$$e_{20}(T)=[(-B_2+\sqrt{B_2^2-4A_2(T)C_2})/(2C_2)]^{1/2}. \tag{4}$$

At the transition temperature T_c, found from $A_2(T_c)=3B_2^2/16C_2$, the three minima $e_2=0$, $\pm e_{20}(T_c)$ are degenerate; here $e_{20}(T_c)=\sqrt{-3B_2/4C_2}$. Finally, the gradient term is responsible for the wall energy; the other derivative invariants[27] are unimportant,[7,12,27] largely because the primary physical spatial dependence is in e_2.

The parameters of the theory are not well known for any material. To reduce the number of unknown parameters, and possibly obtain a universal theory that applies qualitatively to many materials, we transform variables by

$$e_j\rightarrow[e_{20}(T_c)\times 10^3]e_j, \tag{5}$$

$$x_i\rightarrow\sqrt{d_2/A_2(T_c)}x_i, \tag{6}$$

$$\mathcal{F}\rightarrow A_2(T_c)[e_{20}(T_c)\times 10^3]^2\mathcal{F}; \tag{7}$$

also, we define the dimensionless temperature $\tau=A_2(T)/A_2(T_c)=(T-T_0)/(T_c-T_0)$ and dimensionless stiffness parameters $\zeta_1=A_1/A_2(T_c)$ and $\zeta_3=A_3/A_2(T_c)$. The scale factor in Eq. (5) is chosen so that the deviatoric strain at T_c is 10^{-3}, an arbitrary value; the hidden but necessary assumption here is that the strains are small and so the nonlinear term in Eq. (2) can be neglected. The energy density in terms of the new variables is

$$\mathcal{F}=\frac{1}{2}(\zeta_1e_1^2+\tau e_2^2+\zeta_3e_3^2)+\frac{b}{4}e_2^4+\frac{c}{6}e_2^6+\frac{1}{2}(\nabla e_2)^2, \tag{8}$$

where $b=-4\times 10^6$ and $c=3\times 10^{12}$. If temperatures near T_c are accessible, the three parameters in Eq. (8) can be determined from the elastic constants just above T_c, the strain e_2 at T_c, and the T dependence of e_2. For $YBa_2Cu_3O_7$, typical values at low T are[28] an orthorhombic distortion of $2(b-a)/(a+b)=0.017$ (giving $e_{20}=0.012$), and a wall width of ≈ 1.3 nm.

This Landau theory, with all parameters but A_2 assumed independent of T, is in principle restricted in its validity to the immediate vicinity of T_c; the prediction that the homogeneous strain e_{20} does not saturate with decreasing T is particularly doubtful. We note, however, that the primary strain need not saturate rapidly; from Figs. 1.5 and 4.3 of Ref. 2, the strains in lead phosphate ($T_c=453$ K) and As_2O_5 ($T_c=578$ K) are still increasing at room temperature. Whether the simplest Landau theory is adequate at T well below T_c can, it seems, be decided only on a case-by-case basis. We should mention a second weakness of the Landau theory, namely that the use of strain-gradient terms is questionable when the wall width is only a few atomic separations [as in $YBa_2Cu_3O_7$ (Refs. 3 and 28)].

Static structures predicted by Eqs. (3) [or (8)] are discussed in Refs. 6, 8, and 12. Domain walls have lowest energy (e_1 and e_3 are zero) when in the T 110 and $\bar{1}10$ planes. The walls link the variants but also rotate them by an angle proportional to e_2. The rotation, which has no counterpart in conventional order-parameter systems, gives rise to unusual effects when orthogonal walls collide; for example, the visual wall length increases in the collision region, due to variant narrowing[12] resulting from formation of a disclination.

Different structures are found in soft or stiff systems, depending on whether the energy cost is small or large for wall directions off the optimal 110 and $\bar{1}10$ planes. The relevant parameters are the ratios ζ_1/ζ_2 and ζ_3/ζ_2 of the dilatational and shear stiffnesses to the deviatoric stiffness $\zeta_2=\tau+3be_{20}^2+5ce_{20}^4$. The energy cost for wall orientations off

the 110 and $\bar{1}10$ planes increases with both these ratios, though more strongly with ζ_1/ζ_2 it seems. We point out that ζ_2 increases as T decreases, from $\zeta_2=4$ at $\tau=1^-$ to $\zeta_2=238$ at $\tau=-50$, for example. Surprisingly then, in this theory systems should soften as T decreases (we assume that parameters A_1 and A_3 have no strong T dependence). As a result, features like split tips characteristic of stiff systems may disappear on cooling (if the system is moderately stiff just below T_c, low enough temperatures are accessible, and the relaxation is not too sluggish).

B. Time evolution

The Lagrangian density is

$$\mathcal{L}=\mathcal{T}-\mathcal{V}=\frac{1}{2}\rho(\dot{u}_i)^2-\mathcal{F}, \tag{9}$$

where $\dot{u}_i=\partial u_i/\partial t$ and $\mathcal{F}$ is the strain-energy density. To represent the nonconservative forces in the system, we use a Rayleigh dissipative function,[25] with density

$$\mathcal{R}=\frac{1}{2}(A_1'\dot{e}_1^2+A_2'\dot{e}_2^2+A_3'\dot{e}_3^2). \tag{10}$$

This form respects the symmetry of the T phase. The important point is that Eq. (10) leads to dissipative forces that are functions of the spatial derivatives of the velocity, as one would expect, since uniform motion of the material cannot dissipate energy. Then the equations of motion are[25]

$$\rho\ddot{u}_i-\sigma'_{ik,k}-\sigma_{ik.k}=0, \tag{11}$$

where

$$\sigma'_{ki}=\frac{\partial\mathcal{R}}{\partial\dot{u}_{i,k}}, \tag{12}$$

$$\sigma_{ki}=\frac{\partial\mathcal{F}}{\partial u_{i,k}}. \tag{13}$$

The zeroth Fourier component in Eq. (11) should be considered separately since the last two terms are then zero; then the inertial term $\rho\ddot{u}_i$ tells us that the motion is uniform, determined by the initial values.

Effects of the inertial term have been considered previously, for example in Ref. 13. This term is of course important at acoustic-phonon frequencies (say 10^{11} Hz) and it is necessary to describe also rapid domain-wall motion (for example the ''twin cry'' in certain materials). But the frequencies corresponding to domain-wall relaxation are expected to be much smaller and so we neglect the inertial term in the following. By the same argument, the viscosity coefficients A_i' in Eq. (10) are not those measured in ultrasonic attenuation; they are instead effective coefficients appropriate for the mechanisms responsible for domain-wall relaxation. Neglect of the inertial term is occasionally criticized on the grounds that the sound velocity is then in effect infinite; the criticism is quite irrelevant when, as here, the formalism is used only to discuss much slower phenomena.

Equation (11) then simplifies to

$$\sigma'_{ik,k}=-\sigma_{ik,k}. \tag{14}$$

The summation on the index k prevents integration of these equations, except in 1D. In 1D, the constant of integration is crucial, for it represents boundary conditions on the displacement, which may hold the system in a static configuration that is not necessarily the unconstrained minimum of the strain energy.

The equations of motion (14) in terms of the strains are

$$A_1'\dot{e}_{1,1}+A_2'\dot{e}_{2,1}+\frac{A_3'}{\sqrt{2}}\dot{e}_{3,2}=-(G_{1,1}+G_{2,1}+G_{3,2}), \tag{15a}$$

$$A_1'\dot{e}_{1,2}-A_2'\dot{e}_{2,2}+\frac{A_3'}{\sqrt{2}}\dot{e}_{3,1}=-(G_{1,2}-G_{2,2}+G_{3,1}), \tag{15b}$$

where $G_i=\delta\mathcal{F}/\delta e_i$ and the individual functionals are

$$G_1=A_1e_1, \tag{16a}$$

$$G_2=A_2e_2+B_2e_2^3+C_2e_2^5-d_2\nabla^2e_2, \tag{16b}$$

$$G_3=A_3e_3/\sqrt{2}. \tag{16c}$$

We emphasize that our equations of motion (15) are not those of time-dependent Ginzburg-Landau (TDGL) theory. Schematically, the latter are

$$\dot{e}_i\propto-\delta\mathcal{F}/\delta e_i, \tag{17}$$

with a nonlocal expression[29] for the density $\mathcal{F}$; the major difference is the additional space derivatives on both sides of Eq. (15). Equation (17) has much intuitive appeal, not least because it continues the analogy with ferromagnets. Nevertheless, it cannot be correct in principle, and in fact its predictions disagree with those of Eq. (15). We illustrate the point by considering a material with short-range internal forces, uniformly stretched by external forces applied at the ends. When the forces are abruptly released, relaxation begins at the ends and propagates inward, taking a finite amount of time to reach any point in the bulk; the ions (except those near the ends) feel equal but opposite forces from their neighbors until the disturbances reach their vicinity. Equations (15) have the correct behavior, whereas Eq. (17) predicts instantaneous response.

Equations (15) differ also from the dynamics

$$\dot{u}_i\propto-\delta\mathcal{F}/\delta u_i \tag{18}$$

of Refs. 7 and 10, the former at $T=0$. Not having examined physical settings comparable to those where Eq. (18) was used, we cannot compare its results with those of Eq. (15). The right-hand side of Eq. (18) agrees with that of Eq. (14); but the left-hand side, a dissipative force proportional to the velocity, cannot be correct in principle.

From Eqs. (15), the equations of motion for the two components of **u** are

$$\begin{pmatrix} (A_1'+A_2')\partial_1^2+A_3'\partial_2^2/2 & (A_1'-A_2'+A_3'/2)\partial_1\partial_2 \\ (A_1'-A_2'+A_3'/2)\partial_1\partial_2 & (A_1'+A_2')\partial_2^2+A_3'\partial_1^2/2 \end{pmatrix} \begin{pmatrix} \dot{u}_1 \\ \dot{u}_2 \end{pmatrix} = -2\begin{pmatrix} G_{1,1}+G_{2,1}+G_{3,2} \\ G_{1,2}-G_{2,2}+G_{3,1} \end{pmatrix}. \tag{19}$$

By solving these equations, we satisfy automatically the 2D compatibility relation

$$\nabla^2 e_1-(\partial_1^2-\partial_2^2)e_2-\sqrt{8}\partial_1\partial_2 e_3=0 \tag{20}$$

in the small-strain approximation. This necessary and sufficient requirement that the strains be derivable from the displacement can be obtained by starting from $u_{i,12}=u_{i,21}$.

The three viscosity parameters A_i' are not known from experiment, though of course all must be $\geqslant 0$; it is then reasonable to consider the simplest possible theory. In choosing parameter sets, we should avoid those that give a vanishing determinant,

$$\mathrm{Det}=\frac{1}{2}(A_1'+A_2')A_3'(\partial_1^4+\partial_2^4)+[4A_1'A_2'-(A_1'-A_2')A_3']\partial_1^2\partial_2^2 \tag{21}$$

of the coefficients on the left-hand side of Eq. (19); inspection shows that only one of the A_i' can vanish. Other cases of interest are those for which the determinant factors, i.e.,

$$4A_1'A_2'-(A_1'-A_2')A_3'=\pm(A_1'+A_2')A_3', \tag{22}$$

giving three possibilities: (a) $A_1'=0$, (b) $A_3'=2A_2'$, and (c) $A_2'=0$; a fourth, namely $A_3'=-2A_1'$ fails on grounds discussed above. Since e_2 is the primary order parameter, we should keep A_2'; the time scale is then adjusted so that $A_2'=1$. The choices $A_3'=2A_2'$ (the isotropic case) and $A_1'=0$ are convenient, for then the left-hand sides of Eq. (19) decouple. We verified that taking $A_1'=1$ vs $A_1'=0$ has little effect during the evolution; the fully relaxed configurations can differ, however.

We imposed periodic boundary conditions on the displacement **u**, thereby forcing domain walls into the systems; the equilibrium states are a single twin band, optimally with only a pair of walls. We solved Eqs. (19) using a finite-difference, fast-Fourier-transform method. At the beginning of each time step, the displacement field was known at each point of the space grid. Finite-difference approximations (centered on a 5×5 grid) were used to compute the derivatives and so to obtain the right-hand sides in real space. The latter were then Fourier transformed. The Fourier components on the left-hand sides were found using the same finite-difference approximations and then advanced in time using the Euler method (with time step 10^{-5} or so). The results were then Fourier transformed back to real space to begin the next step.

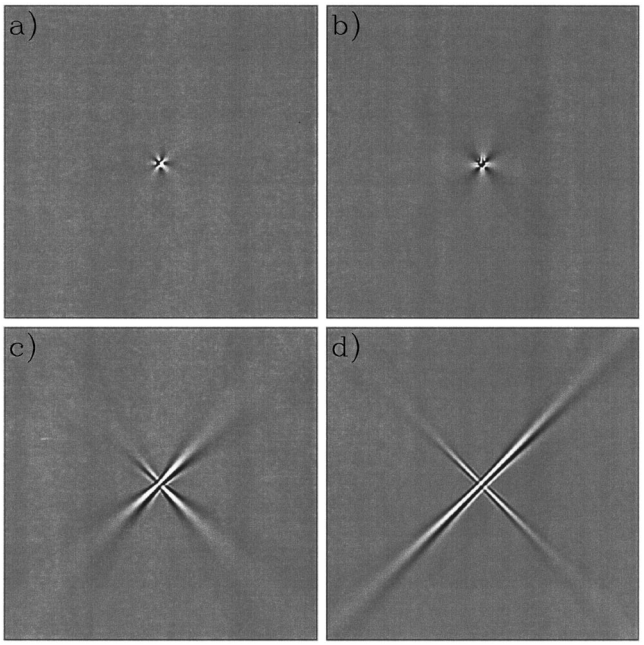

FIG. 1. Greyscale snapshots of orthorhombic (*O*) nuclei growing after identical perturbations of the supercooled tetragonal (*T*) phase. The two *O* variants are white and black, the *T* matrix grey. Parts (a) and (b) show soft systems ($\zeta_1=1$) with $\zeta_3=1$ and 1000, respectively; parts (c) and (d) show moderately stiff systems ($\zeta_1=1000$), again with $\zeta_3=1$ and 1000, respectively. All four snapshots are at the same time $t=0.18$ following the nucleation event.

III. T-O NUCLEUS IN TWO DIMENSIONS

This section studies the nucleus resulting from perturbing the supercooled T phase in various ways. All results are for a grid of 512×512 points, with step size 0.4.

We first present results obtained by displacing a single point off a high-symmetry direction. Figure 1 shows snapshots for $\tau=-50$ ($\zeta_2=238$) and for four sets of values of ζ_1 and ζ_3, all at time $t=0.18$ after identical nucleation events; the viscosity parameters are $A_1'=0$, $A_2'=1$, and $A_3'=2$. Figure 2 shows snapshots of the same systems at the later time $t=0.24$. Very little is known about the relative importance of the stiffnesses ζ_1 and ζ_3 and so we investigated some extreme cases; we find stronger dependence on ζ_1 than on ζ_3. Parts (a) and (b) of Figs. 1 and 2 show soft systems ($\zeta_1=1$), with $\zeta_3=1$ and 1000, respectively, whereas parts (c) and (d) show moderately stiff systems ($\zeta_1=1000$), again with $\zeta_3=1$ and 1000, respectively. The important point is that the nucleus has very different shapes in soft and stiff systems; one notes also the more rapid growth in the latter.

In the soft systems, the domain walls lie off the optimal directions; the nucleus retains its flower shape as it expands. In the stiff systems, the domain walls are much closer to the optimal orientations. The nucleus has a striking X shape with arms in the 110 and $\bar{1}10$ directions; growth transverse to the arms results from the appearance of new variants near the nucleation site and their subsequent growth along the arms.

Other sets of simulations started from point displacements in high-symmetry directions (100 and 110), and others from displacements of small areas. Every soft system gave a

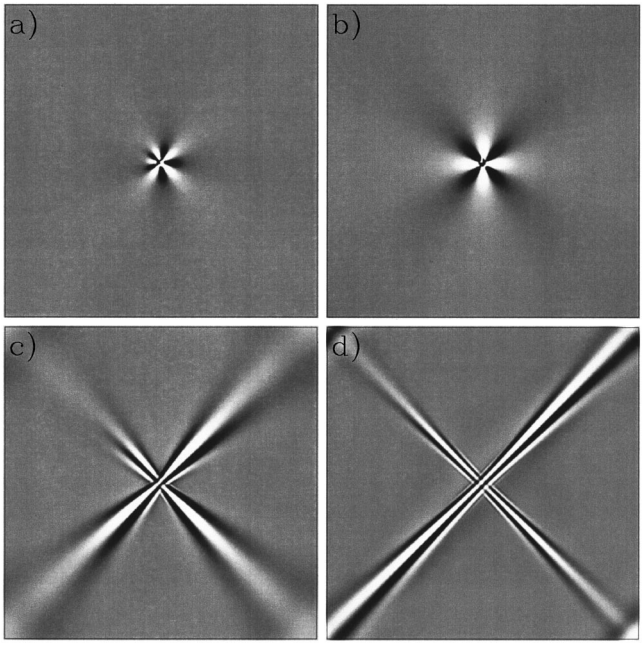

FIG. 2. The nuclei of Fig. 1 at a later time $t=0.24$.

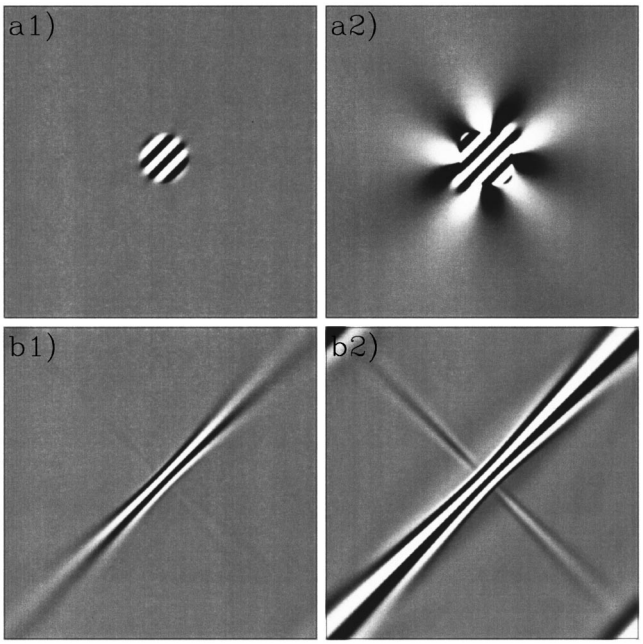

FIG. 3. Snapshots of *O* nuclei growing in a *T* matrix, for (a) soft and (b) stiff parameters. The dimensions of the two systems are identical. The starting configuration for both was a circular region of twinned *O* material; the area was about one-fourth smaller in (b). Parts (a1) and (a2) show the nucleus at times 0.12 and 0.24 for a soft system ($A_1'=0$, $A_2'=1$, $A_3'=2$, $\zeta_1=\zeta_3=1$, $\tau=-50$); the earlier snapshot shows little change from the starting configuration, whereas the later shows growth in both 110 and $\bar{1}10$ directions. Parts (b1) and (b2) show the nucleus at times 0.12 and 0.18 for a stiff system ($A_1'=0$, $A_2'=1$, $A_3'=2$, $\zeta_1=\zeta_3=1000$, $\tau=-50$). The circular region is unstable in both cases; the soft system evolves toward the flower pattern in Figs. 1 and 2, and the stiff system toward the corresponding X pattern.

flower with eight or more distinct domains emanating from the disturbed area; every stiff system gave the X shaped nucleus.

Yet more sets of simulations started from circular regions containing several parallel stripes in one direction. The intention was in part to examine the stability, under our dynamics, of a nucleus like that found in Ref. 11 using TDGL dynamics; we must point out, however, that our simulations and those of Ref. 11 differ in respects other than the dynamics. We find that the circular regions are unstable in both soft and stiff systems, that they evolve rapidly to configurations much like those (described above) resulting from point perturbations. Figures 3(a1) and 3(a2) show the growth process for a soft system; the nucleus grows longitudinally (parallel to the stripes), but also transversely, developing side lobes and so evolving toward the flowerlike patterns in Figs. 1(a) and 1(b) and 2(a) and 2(b). Figures 3(b1) and 3(b2) show the evolution of a stiff system. The faster growth occurs in the longitudinal direction, but twinned jets shoot out transversely, thereby evolving the system toward the X shape in Figs. 1(c) and 1(d) and 2(c) and 2(d). The two sets of jets are more asymmetric here, because the rapid longitudinal growth exaggerates the greater asymmetry in the starting configuration. Nevertheless, it is clear that even this starting configuration is also unstable toward the formation of perpendicular jets and evolution to the X shape. For both systems, we find that growth is primarily along the 110 and $\bar{1}10$ directions; growth in the 100 and 010 directions is slow.

Simulations at temperatures between $\tau=-100$ and $\tau=-5$ gave results qualitatively similar to those described in Figs. 1–3; the major difference is that the nucleus grows more slowly at higher *T*, as expected. The important point is that the flower/X shapes were found for soft/stiff systems at all *T*. We were unable to nucleate the low-*T* phase above $\tau=-5$ (well below the stability limit $\tau=0$ of the T phase) and so we could not examine the parameter set of Ref. 11.

Because the gross features are independent of the starting configurations and temperature, we believe that we have found the nucleus of the T-O transformation in 2D, at least below $\tau=-5$. Application should be immediate to thin films, and it is reasonable to expect that x-y cuts through the 3D T-O nucleus will resemble our 2D nucleus.

None of our simulations (with any starting configuration, with either soft or stiff parameters, at any temperature) gave a nucleus resembling that found using TDGL theory in the strains. The 2D T-O nucleus of Ref. 11 accords with one's intuition based on conventional systems. It is compact, elliptical in shape (with axes along the 110 and $\bar{1}10$ directions), and internally twinned (with walls parallel to the major axis); the twinning generates both positive and negative displacements which largely cancel overall. Transverse growth occurs by adding walls and variants, whereas existing variants grow only longitudinally. Although other aspects are different (Ref. 11 studied soft systems, used a somewhat different strain-energy functional, and worked at higher *T*, namely $\tau=0.3$), it is likely that the different results reflect the different dynamics.

None of our simulations gave a nucleus like that in the

more phenomenological study of Ref. 22, namely growth to an untwinned square which then flowers.

To our knowledge, the only previous use of the equations of motion (14) to examine nucleation was in a study of H-O ferroelastics;[17] these systems are dominated by disclinations. In soft systems the nucleus is flowerlike, as in T-O systems, but has 12 arms; in stiff systems it branches early in the growth, without forming the long arms seen above in T-O systems.

IV. COARSENING

This section studies the coarsening phenomena that occur after completion of the phase transition. The most interesting feature is that we find behavior very different from that observed in conventional order-parameter systems; although the deviatoric strain is a conventional order parameter at the level of the Landau free-energy expansion, the compatibility relations, combined with the dilatational and shear energies, deny the utility of guides such as total wall length in predicting the time evolution.

Simulations started from systems with orthogonal twin bands, relaxed internally but not in the collision regions. The initial relaxation from these artificial high-energy configurations is rapid and of no interest; we present results at later times, but well before equilibrium is reached.

Figure 4 shows four pairs of snapshots. Parts (a) to (c) are for soft systems with different initial conditions, all with parameters $A_1'=A_2'=A_3'=1$, $\zeta_1=\zeta_3=10$, and $\tau=-50$; the times between the pairs are 0.5, 0.5, and 1.0, respectively. In part (a), the island at the center vanishes, but other islands form as some narrow domains pinch off and retract. In part (b), one tip retracts to form rank with its neighbor; at the lower right, other tips retract in unison, keeping the rank. In part (c), coarsening occurs by different kinds of coordinated events; domain merges parallel to the smaller-scale patterns occur at the top left and perpendicular at the bottom right. Part (d) corresponds to a stiffer system, with parameters $A_1'=A_2'=1$, $A_3'=2$, $\zeta_1=\zeta_3=500$, and $\tau=-100$ ($\zeta_2=452$); the time difference is 0.6. The patterns are strikingly similar to published transmission electron-microscopy pictures of $YBa_2Cu_3O_7$, particularly Figs. 7.9 and 7.17(b) of Ref. 2 [and to a lesser extent Fig. 2(b) of the second part of Ref. 3]. One sees the formation of a split tip and also the counterintuitive variant narrowing and wall wobbling found in the static theory.[12] Related theories of needle twins and tip splitting are given in Refs. 30 and 31.

The observation of tip splitting[2,3] in $YBa_2Cu_3O_7$ suggests that this material is moderately stiff ($\zeta_1 \gtrsim \zeta_2$) at the temperatures investigated. Values of the elastic constants suggest that Fe-Pd alloys (cubic-tetragonal) are also moderately stiff.[16]

These coarsening phenomena, like the nucleation phenomena reported in Sec. III, confound intuition based on conventional order-parameter systems. The relaxation cannot be characterized by any simple rules; that is, the changes from one snapshot to the next cannot be predicted by inspection of the strain patterns alone. The visible domain-wall length often increases. The relaxation is nonlocal;[29] rapid changes occur in one part of the system while other parts, with no apparent major differences from the first, stay almost unchanged. The tendency is toward coarser patterns, but occasionally the topology becomes more complicated (as when islands form). The ribbons seldom retract immediately, even though retraction reduces the wall length. Particularly strange are the rank formation of tips and their linked withdrawal, the variant narrowing and the splitting of tips. Transverse wall motion occurs only locally, for example in the process of pinching off the other variant.

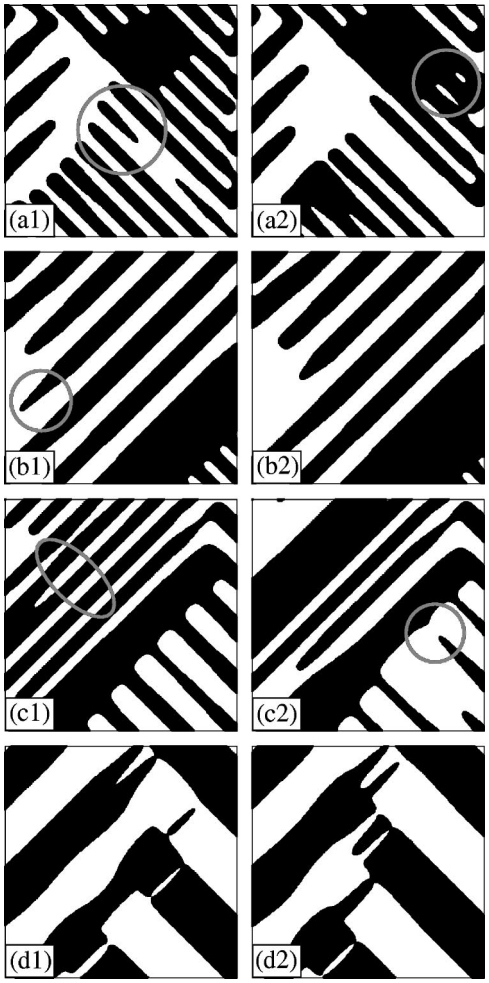

FIG. 4. Pairs of snapshots showing the time evolution of structures for four different initial conditions or parameter sets. Each part is a 128×128 piece of a full 256×256 simulation with step size 0.2. Parts (a) to (c) are soft systems ($\zeta_1=\zeta_3=10$) and part (d) stiff ($\zeta_1=\zeta_3=500$). The times between the pairs are $t=0.5$, 0.5, 1.0, and 0.6, respectively.

Our simulations resemble in some respects those of Refs. 20, 23, and less those of Refs. 18, 9, 11. Coarsening mechanisms in simulations of H-O systems,[17] also using Eqs. (14), differ from those in Fig. 4 (again due to the disclinations in H-O systems).

V. SUMMARY

We have derived general equations of motion for proper T-O ferroelastics including inertia, dissipation, and internal elastic stress. These equations, and more importantly their

predictions, differ from those of all previous studies of proper T-O ferroelastics. We studied the growth of the O nucleus for both soft and stiff systems, in 2D. Soft systems grow with time like a flower, while stiff systems assume a characteristic X shape, with twinning along the arms. We studied also the coarsening mechanisms that relax the O phase toward local equilibrium, again in 2D. We observed the formation and disappearance of island domains, tip retraction and domain merging, both parallel and perpendicular to existing domain walls; in stiff systems we observed the formation of split tips. Because the time scale is expected to be short, it will likely be difficult to observe details of the time evolution in proper ferroelastics; as discussed above, however, our results are consistent with patterns in quenched samples. Details of the time evolution may be observable in improper systems, where the time scale may be longer. Again, our strain-only theory does not apply in principle to improper ferroelastics, but it explains many puzzling features of patterns reported in Refs. 2 and 3, and so perhaps it can shed light on the dynamics also.

The above treatment should be extended to include thermal noise. Without noise, the system cannot surmount energy barriers during the relaxation stage, we cannot describe the tweed structure (which perhaps requires also compositional inhomogeneities) and we cannot address issues related to the early stages of nucleation such as the size, shape, kinetics, and energetics of the critical nucleus. For reasons discussed above however, we believe that we have found the nucleus in its growth stage (perhaps though only at lower T).

The primary need in the field is, however, *in situ* observations of the dynamics in T-O systems; these are difficult and correspondingly rare. The available studies[31,32] cannot decide the relative merits of the many theories.

ACKNOWLEDGMENTS

This research was supported by the Natural Sciences and Engineering Research Council of Canada. We are grateful to E. K. H. Salje, R. C. Desai, and V. Heine for discussions.

*Present address: Institute for Solid State Physics, University of Tokyo, Kashiwa-no-ha 5-1-5, Kashiwa, Chiba 277-8581, Japan. Electronic address: curnoe@issp.u-tokyo.ac.jp

†Electronic address: jacobs@physics.utoronto.ca

[1] K. Aizu, J. Phys. Soc. Jpn. **27**, 387 (1969).

[2] E. K. H. Salje, *Phase Transitions in Ferroelastic and Co-elastic Crystals* (Cambridge University Press, Cambridge, England, 1993).

[3] A. H. King and Y. Zhu, Philos. Mag. A **67**, 1037 (1993); Y. Zhu, M. Suenaga, and J. Tafto, *ibid.* **67**, 1057 (1993).

[4] F. Falk, Z. Phys. B **51**, 177 (1983).

[5] G. R. Barsch and J. A. Krumhansl, Phys. Rev. Lett. **53**, 1069 (1984).

[6] A. E. Jacobs, Phys. Rev. B **31**, 5984 (1985).

[7] S. Kartha, T. Castán, J. A. Krumhansl, and J. P. Sethna, Phys. Rev. Lett. **67**, 3630 (1991); S. Kartha, J. A. Krumhansl, J. P. Sethna, and L. K. Wickham, Phys. Rev. B **52**, 803 (1995).

[8] A. E. Jacobs, Phys. Rev. B **52**, 6327 (1995).

[9] W. C. Kerr, M. G. Killough, A. Saxena, P. J. Swart, and A. R. Bishop, Phase Transit. **69**, 247 (1999).

[10] A. Onuki, J. Phys. Soc. Jpn. **68**, 5 (1999).

[11] S. R. Shenoy, T. Lookman, A. Saxena, and A. R. Bishop, Phys. Rev. B **60**, 12 537 (1999).

[12] A. E. Jacobs, Phys. Rev. B **61**, 6587 (2000).

[13] A. C. E. Reid and R. J. Gooding, Phys. Rev. B **50**, 3588 (1994), and references therein.

[14] P. Klouček and M. Luskin, Continuum Mech. Thermodyn. **6**, 209 (1994); Math. Comput. Modell. **20**, 101 (1994).

[15] K. Ø. Rasmussen, T. Lookman, A. Saxena, A. R. Bishop, and R. C. Albers, cond-mat/0001410 (unpublished).

[16] S. H. Curnoe and A. E. Jacobs, Phys. Rev. B **62**, R11 925 (2000).

[17] S. H. Curnoe and A. E. Jacobs, Phys. Rev. B **63**, 094110 (2001).

[18] S. Semenovskaya and A. G. Khachaturyan, Phys. Rev. Lett. **67**, 2223 (1991); Phys. Rev. B **46**, 6511 (1992).

[19] S. Semenovskaya, Y. Zhu, M. Suenaga, and A. G. Khachaturyan, Phys. Rev. B **47**, 12 182 (1993), and references therein.

[20] A. M. Bratkovsky, V. Heine, and E. K. H. Salje, Philos. Trans. R. Soc. London, Ser. A **354**, 2875 (1996), and references therein.

[21] A. Saxena, Y. Wu, T. Lookman, S. R. Shenoy, and A. R. Bishop, Physica A **239**, 18 (1997).

[22] Y. Yamazaki, J. Phys. Soc. Jpn. **67**, 2970 (1998).

[23] T. Ichitsubo, K. Tanaka, M. Koiwa, and Y. Yamazaki, Phys. Rev. B **62**, 5435 (2000), and references therein.

[24] Y. H. Wen, Y. Wang, and L. Q. Chen, Acta Mater. **47**, 4375 (1999); Philos. Mag. A **80**, 1967 (2000).

[25] H. Goldstein, *Classical Mechanics*, second edition (Addison-Wesley, Reading, MA, 1980); L. D. Landau and E. M. Lifshitz, *Theory of Elasticity* (Oxford University, New York, 1986).

[26] A. C. E. Reid and R. J. Gooding, Physica A **239**, 1 (1997).

[27] A. E. Jacobs, Phys. Rev. B **46**, 8080 (1992).

[28] Z.-X. Cai and Y. Zhu, *Microstructures and Structural Defects in High-Temperature Superconductors* (World Scientific, River Edge, NJ, 1998).

[29] Eliminating the displacement in a way that satisfies the compatibility relations generates an anisotropic, oscillatory, and long-range interaction between primary strains at different locations. The interaction provides insight into the nonlocal relaxation and other unusual phenomena in ferroelastics (such as wall wobbling). Such treatments go back well before A. G. Khachaturyan, *The Theory of Structural Transformations in Solids* (Wiley, New York, 1983). Recent treatments for proper ferroelastics are given in Refs. 7,9,11, and 15. Long-range interactions appear also in Refs. 18–24.

[30] R. V. Kohn and S. Müller, Philos. Mag. A **66**, 697 (1992).

[31] E. K. H. Salje, A. Buckley, G. Van Tendeloo, Y. Ishibashi, and G. L. Nord, Jr., Am. Mineral. **83**, 811 (1998).

[32] G. Van Tendeloo, H. W. Zandbergen, and S. Amelinckx, Solid State Commun. **63**, 389 (1987).